Experimental detection of the CNO cycle

B. Caccianiga[1], N. Rossi[2], G. Testera[3]
M. Agostini, K. Altenmüller, S. Appel, V. Atroshchenko, Z. Bagdasarian, D. Basilico, G. Bellini, J. Benziger, R. Biondi, D. Bravo, B. Caccianiga, F. Calaprice, P. Cavalcante, A. Chepurnov, D. D'Angelo, S. Davini, A. Derbin, A. Di Giacinto, V. Di Marcello, X.F. Ding, A. Di Ludovico, L. Di Noto, I. Drachnev, A. Formozov, D. Franco, C. Galbiati, C. Ghiano, M. Giammarchi, A. Goretti, A.S. Göttel, M. Gromov, D. Guffanti, Aldo Ianni, Andrea Ianni, A. Jany, D. Jeschke, V. Kobychev, G. Korga, S. Kumaran, M. Laubenstein, E. Litvinovich, P. Lombardi, I. Lomskaya, L. Ludhova, G. Lukyanchenko, L. Lukyanchenko, I. Machulin, J. Martyn, E. Meroni, M. Meyer, L. Miramonti, M. Misiaszek, V. Muratova, B. Neumair, M. Nieslony, R. Nugmanov, L. Oberauer, V. Orekhov, F. Ortica, M. Pallavicini, L. Papp, L. Pelicci, Ö. Penek, L. Pietrofaccia, N. Pilipenko, A. Pocar, G. Raikov, M.T. Ranalli, G. Ranucci, A. Razeto, A. Re, M. Redchuk, A. Romani, N. Rossi, S. Schönert, D. Semenov, G. Settanta, M. Skorokhvatov, A. Singhal, O. Smirnov, A. Sotnikov, Y. Suvorov, R. Tartaglia, G. Testera, J. Thurn, E. Unzhakov, F. Villante, A. Vishneva, R.B. Vogelaar, F. von Feilitzsch, M. Wojcik, M. Wurm, S. Zavatarelli, K. Zuber, and G. Zuzel

[1] *Dipartimento di Fisica, Università degli Studi e INFN, 20133 Milano, Italy*

[2] *INFN Laboratori Nazionali del Gran Sasso, 67010 Assergi (AQ), Italy*

[3] *Dipartimento di Fisica, Università degli Studi e INFN, 16146 Genova, Italy*

The Borexino has recently reported the first experimental evidence of neutrinos from the CNO cycle. Since this process accounts only for about 1% of the total energy production in the Sun, the associated neutrino flux is extremely low as compared with the one from the pp-chain, the dominant process of hydrogen burning. This experimental evidence of the CNO neutrinos was obtained using the highly radio-pure liquid scintillator of Borexino. Improvements in the thermal stabilization of the detector over the last five years enabled us to exploit a method to constrain the rate of ^{210}Bi background. Since the CNO cycle is dominant in massive stars, this result gives the first experimental proof of the primary mechanism for stellar conversion of hydrogen into helium in the Universe.

Keywords: Solar neutrinos, CNO cycle, Liquid organic scintillators, solar models

Introduction

Stars are fuelled by nuclear fusion of light elements with a release of an enormous amount of energy. In particular the *pp* chain and the CNO cycle, active also in the Sun, produces a rich spectrum of electron-flavour neutrinos detectable on the Earth.[1,2] Those two mechanisms basically converts four hydrogen nuclei into a helium nucleus: the first using direct process throughout a big variety of branches, while the second using a closed loop starting and ending with ^{12}C acting as catalyst.

The contribution of these two mechanisms in the energy production is related to mass, and then to the core temperature, of the stars and to abundance of elements heavier than helium in the core (in jargon, "metallicity").

For stars heavier than 1.3 $M_\odot$ the CNO cycle is the dominant process of hydrogen fusion,[3] while in the Sun, with a core temperature of about 15×10^6K, the CNO accounts only for 1% of the total luminosity, with a large uncertainty related to poorly known metallicity.[4] The Borexino experiment, starting from mid-2007, has published a comprehensive study of the neutrino from the *pp* chain [5] and recently has reported the first direct detection of the CNO.[26] The CNO quest, started by Borexino, could in principle create a situation that makes it possible the solution of the long standing "solar metallicity problem" ,[2] i.e. the disagreement between the metallicity predicted by solar models using updated (low) metal abundances from spectroscopy (SSM-LZ) [6] and the one obtained from the helioseismology, which foresees a higher metal content (SSM-HZ).

In Sec. 1 a description of the detector and the main physics results of Borexino are reported. At the end of the section the hardware improvement for the CNO detection in Phase-III is also reported. In Sec. 2 the main strategy for the CNO detection is described and in Sec. 3 the independent constraint of the ^{210}Bi (the main background for the CNO neutrino interaction rate) is largely detailed. Finally, in Sec. 4 the spectral analysis for the extraction of the CNO rate in Borexino is presented.

1. The Borexino detector

Borexino experiment is the only experiment capable to detect solar neutrinos with a threshold as low as about 150 keV and to reconstruct the position and the energy of each event in real-time.

Borexino is located in the Hall C of Laboratori Nazionali Gran Sasso (INFN).[12] The detector is made of concentric shells with increasing radiopurity (see e.g. Ref.[13]): the innermost core, enclosed in a 125 μm thick ultra-pure nylon vessel of radius 4.25 m, is made of 300 tons of liquid scintillator (1,2,4-Trimethylbenzene with 1.5 g/l of PPO wavelength shifter). The active core is contained by a stainless steel sphere filled up with $\sim$ 1000 of buffer liquid (1,2,4-Trimethylbenzene with DMP quencher), whose internal surface is instrumented with more than 2000 PMTs for detecting the scintillation light. Finally, the SSS is located inside a 2000 ton water Cherenkov detector, equipped with about 200 PMTs. In Fig. 1 all the parts described above are represented in a graphical scheme. Thanks to an intense calibration campaign carried out in 2010, the Borexino detector is able to reconstruct the event position with an accuracy of ~ 10 (at 1 MeV) and with energy resolution of about $\sigma(E)/E = 5\%/\sqrt{(E/[MeV])}$.

The Borexino data-set is traditionally divided in three Phases, determined by the hardware milestones: Phase-I, from mid-2007 to beginning of 2010, ended with the calibration campaign, in which the first measurement of the ^{7}Be solar neutrino interaction rate[8–10] was performed; Phase-II, from the-beginning of 2012 to mid-2016, started after an intense purification campaign, based on water extraction, with unprecedented suppression of the radioactive contaminants, in which the first

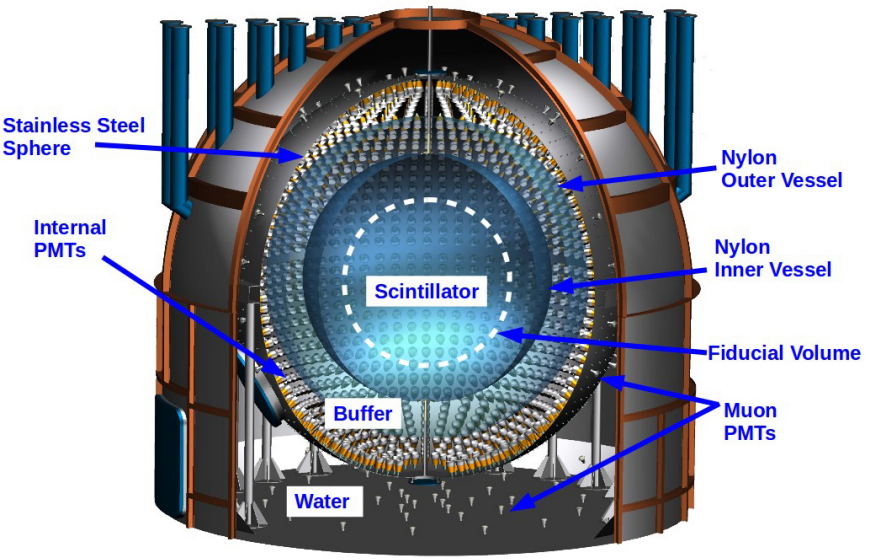

Fig. 1. Scheme of the Borexino detector.

evidence of the *pep* neutrinos[15] and a 10% measurement of the *pp* neutrinos[16] were published, later updated in the solar neutrino comprehensive analysis;[17–19] Phase-III, from mid-2016 to 2021 (still in progress), after the thermal insulation program, in which the first detection of the CNO neutrinos[11] discussed here was performed. Table 1 summarizes the most important results concerning solar neutrinos interaction rates measured by Borexino. Thanks to its unprecedented radio-purity, Borexino has also set a lot of limits on rare processes (see e.g.,[20–24] and performed other neutrino physics studies, as e.g. geo-neutrino detection (for review, see e.g.[25])

The CNO detection has required, as it is explained in Sec. 2, an independent constraint of the ^{210}Bi contaminant from the ^{210}Po through the secular equilibrium starting from the out-of-equilibrium parent ^{210}Pb, present in the liquid scintillator

Table 1. Solar neutrino interaction rates and fluxes measured by Borexino. Rates are reported in cpd/100t, while fluxes are reported in cm^{-2}s^{-1}.

Species	Rate [cpd/100t]	Flux [cm^{-2} s^{-1}]
pp	$(134 \pm 10)^{+6}_{-10}$	$(6.1 \pm 0.5)^{+0.3}_{-0.5} \times 10^{10}$
^{7}Be	$(48.3 \pm 1.1)^{+0.4}_{-0.7}$	$(4.99 \pm 0.11)^{+0.06}_{-0.08} \times 10^{9}$
pep (HZ)	$(2.7 \pm 0.4)^{+0.1}_{-0.2}$	$(1.3 \pm 0.3)^{+0.1}_{0.1} \times 10^{8}$
^{8}B($>$ 3 MeV)	$0.223^{+0.021}_{-0.022}$	$5.68^{+0.42}_{-0.44} \times 10^{6}$
CNO	$7.2^{+3.0}_{-1.7}$	$7.0^{+3.0}_{-2.0} \times 10^{8}$
hep	< 0.002 (90% CL)	$< 1.8 \times 10^{5}$ (90% CL)

after the purification carried out at the end of Phase-I. That constraint required the contaminants, and then the whole scintillator, to be stable against the the convective motions activated by the seasonal variation of the temperature in the experimental hall hosting the detector. In mid-2014 Borexino was equipped with a detailed temperature mapping. In mid-2015 the detector was covered with a thermal insulation and, from the beginning of 2016, a series of active temperature control system were installed around the water tank and at the end on the experimental hall. See for details Ref.[26].

The thermal insulation program was aimed at the realization of a vertical temperature gradient from the cold floor, made of constant temperature rock with a huge thermal capacitance, and the detector top, warmed up by the air flushed into the underground laboratory coming from the external environment out of the Gran Sasso mountain. This challenging enterprise was successful and the strongest convective motions, mixing the liquid scintillator and then the contaminants from the outermost regions into the center, were actually stopped and the conditions for the ^{210}Bi-^{210}Po link, described in Sec. 3 were finally met. Figure 2 shows the ^{210}Po contaminant evolution during the thermal insulation program in 59 small cubes enumerated from the bottom to the top inside a radius of 3 m from the center of the Inner Vessel. The red superimposed curve represents the average temperature in the same region. The dashed vertical lines show the most important milestones of the temperature stabilisation program: 1. Beginning of insulation; 2. Turning off of the water recirculation system in the Water Tank; 3. First operation of the active temperature control system; 4. Change of the active control set point; 5. Installation and commissioning of the Hall C temperature control system. The white vertical bands represent different technical DAQ breaks. The ^{210}Po shown in the figure is a

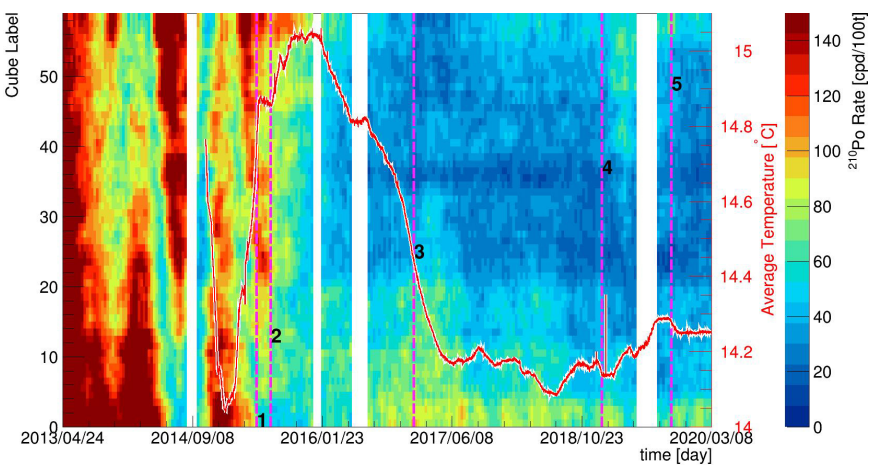

Fig. 2. Evolution of the ^{210}Po contamination during the thermal insulation program.

tracker of the convective motions, that are drastically damped as a consequence of the insulation program.

2. CNO detection strategy

Neutrinos emitted in the CNO cycle, see Fig. 3, have a continuous spectrum with a maximum energy of 1.74 MeV (see Fig. 4, left). In the Sun, the flux of CNO neutrinos is two orders of magnitude smaller than the one due to proton-proton neutrinos: this makes the expected rate in Borexino very low, of the order of few counts per day. Besides the low rate, the main difficulty in detecting CNO neutrinos with Borexino is the presence of two radioactive backgrounds which produce signal in approximately the same energy region: ^{11}C and ^{210}Bi. Furthermore, also solar neutrinos from the *pep* reaction are a significant background for the CNO analysis.

Fig. 4 (right) shows a MonteCarlo simulation of the energy spectrum of electrons scattered by neutrinos from the CNO cycle (red line) in comparison with the signal induced by the radioactive decay of ^{11}C (purple line) and ^{210}Bi (green line). The blue line is the *pep* signal. The relative proportion of the four contributions is approximately the one expected in reality. From this plot the difficulty of extracting the CNO signal from the background becomes evident: it is like looking for a needle in a haystack!

The cosmogenic ^{11}C is an isotope produced by residual muons crossing the scintillator which decays emitting a positron with a lifetime of approximately 30 minutes. It can be very effectively tagged by the Three Fold Coincidence (TFC) method described in,[27] which looks for the triple coincidence of the parent muon, the cosmogenic neutron produced together with ^{11}C and the positron emitted in the ^{11}C decay. This tagging method allows us to divide the data-set in two complementary parts, one rich and the other depleted in ^{11}C which are then simultaneously fitted in the multivariate analysis described in Section 4. This is a powerful tool to help the fit isolate the ^{11}C signal contribution, breaking the correlation with the CNO neutrino signal.

Separating the CNO signal from the ^{210}Bi and *pep* one is more tricky since their spectral shapes are quite similar and the multivariate fit has trouble in distinguishing between them, if no additional external contraints are imposed.

For what concerns *pep* neutrinos, we exploited the external and independent information coming from the available solar neutrino data, solar luminosity and the most recent oscillation parameters to put a constraint to their rate in the fit with a 1.4% uncertainty.

The remaining obstacle to the CNO neutrino detection is the contamination from ^{210}Bi. This isotope belongs to the ^{210}Pb chain, which in turn is the last segment of the ^{238}U chain. In Borexino, we found the ^{210}Pb chain to be out of equilibrium with respect to the ^{238}U chain and with a significantly higher activity, of the order of tens of counts per day per 100 tons of scintillator.

The ^{210}Pb chain is composed of three isotopes: the long lived ^{210}Pb father of the chain ($\tau \sim 32\,\mathrm{y}$), ^{210}Bi which has a relatively short lifetime ($\tau \sim 7.23\,\mathrm{d}$) and ^{210}Po which decays into ^{206}Pb (stable) emitting an alpha particle ($\tau \sim 199.1\,\mathrm{d}$). If secular equilibrium holds, the activities of ^{210}Bi and ^{210}Po are the same (apart for negligible corrections due to the finite ^{210}Pb lifetime). Measuring the ^{210}Po rate is in principle straightforward since an alpha peak is clearly separable from the continuous beta-like background underneath. Furthermore, alpha/beta discrimination techniques provide a powerful additional tool to isolate the ^{210}Po events.

Based on these premises, our strategy for the CNO detection relies on the ^{210}Bi - ^{210}Po link to determine independently the ^{210}Bi content from ^{210}Po and constrain it in the multivariate fit. The next Section will describe in details the difficulties we encountered to apply this technique and how we were able of overcoming them.

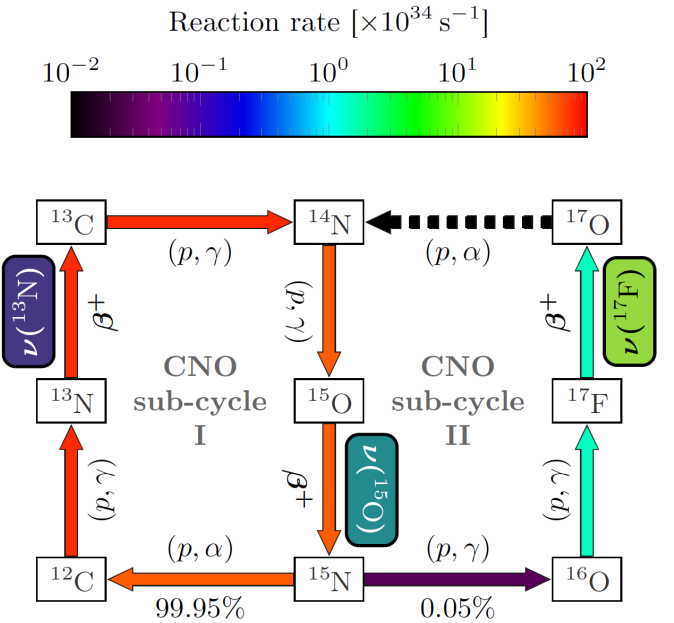

Fig. 3. Neutrinos in CNO cycle.

3. The ^{210}Bi–^{210}Po link

In order to exploit the ^{210}Bi–^{210}Po link to obtain an external constraint on the ^{210}Bi rate, we carefully studied the evolution in time and the spatial distribution

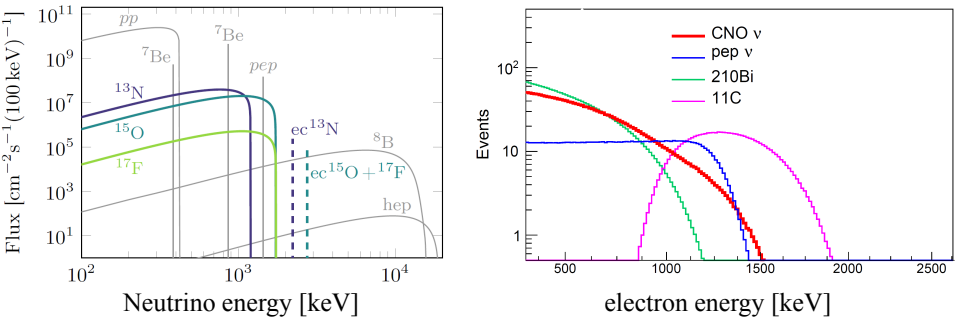

Fig. 4. (Left): Energy spectrum of neutrinos emitted in the CNO cycle (colored lines); (right): energy spectrum in Borexino for events of CNO (red), *pep* (blue), $^{@10}$Bi (geen) and ^{11}C (purple) obtained from MonteCarlo simulations.

of the polonium contamination in the detector during the Borexino data-taking. We soon realized that the ^{210}Po present in the fiducial region used in the analysis (an innermost subset of the scintillator volume) is actually the sum of two contributions: ^{210}Po from the intrinsic ^{210}Pb scintillator contamination (in equilibrium with ^{210}Bi); ^{210}Po from the nylon vessel containing the scintillator. This last contribution was found to be changing in time and highly correlated with variations of the temperature gradient in the detector, which induce convective motions strong enough to bring ^{210}Po from the vessel surface into the fiducial region. In order to reduce these convective motions, we thermally insulated the detector, as discussed in Section 1.

After the completion of the thermal insulation (2016), the temperature of the detector has become very stable and the convective currents inside the scintillator have significantly reduced. This has favoured the formation of an innermost region of the detector, called Low Polonium Field (LPoF), where the contribution to the ^{210}Po rate coming from the vessel is very small. A pictorial view of this region is shown in Fig. 5. This region exhibits an effective migration profile with a minimum in the ^{210}Po rate above the detector equator (dark blue region). The qualitative shape and approximate position of the LPoF is reproduced by fluid dynamical numerical simulations reported in .[28]

Assuming azimuthal symmetry around the detector z-axis (which was confirmed by a 3D analysis), the ^{210}Po minimum activity is determined by fitting LPoF with a 2D paraboloidal function:

$$\frac{d^2R(^{210}\mathrm{Po})}{d(\rho^2)dz} = \left[R(^{210}\mathrm{Po_{min}})\epsilon_{\mathrm{E}}\epsilon_{\mathrm{MLP}} + R_\beta\right] \times \times \left(1 + \frac{\rho^2}{a^2} + \frac{(z-z_0)^2}{b^2}\right), \quad (1)$$

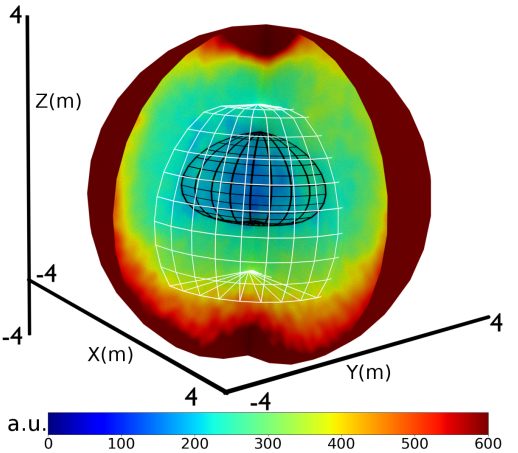

Fig. 5. Pictorial view of the ^{210}Po activity in the Borexino scintillator. The color scale goes from red (highest activity) to blue (lowest activity). The LPoF is the innermost blue region where the contribution of ^{210}Po from the vessel is the smallest (black grid). The white grid indicates the software defined fiducial volume used for the analysis to extract the CNO neutrinos.

Here, $\rho^2 = x^2 + y^2$, a and b are the paraboloid axes, z_0 is the position of the minimum along the z axis, $\epsilon_{\rm E}$ and $\epsilon_{\rm MLP}$ are the efficiencies of the cuts used to select ^{210}Po events, and R_β is the residual rate of β events after the selection. First, we performed the fit integrating data from 2 months (compatible results are obtained also changing the time bins) and we found that the minimum position slowly moves along the z direction by less than 20 cm per month. In order to perform a better estimation of the ^{210}Po minimum, we finally sum up all the time bins after aligning the 3D distributions with respect to z_0.

From this fit we extract the ^{210}Po minimum. This value might still have a small contribution from the vessel component, therefore this method provides only an upper limit for the ^{210}Bi rate. In order to cross-check the results, we performed the fit in different ways: adopting a standard likelihood fit with ROOT or a Bayesian tool called MultiNest. In addition to the 2D paraboloidal fit, we also performed the fit with a 3D ellipsoidal function or alternatively with a cubic spline. The differences in the results were included in the systematic error associated to the upper limit on ^{210}Bi. In the analysis to extract the CNO neutrino rate which will be described in Section 4, we would like to costraint the value of the ^{210}Bi to the upper limit found in the low polonium field region, extrapolating the results to the whole fiducial volume. In order to do so, we need to verify that ^{210}Bi is uniform in this volume during the time period over which the estimation is performed. For this reason, we studied the spatial distribution of β-like events in an energy window where the bismuth contribution is maximized. This distribution was found to be uniform within errors: we include in the systematic error budget a contribution of 0.78 cpd/100t accounting for residual non uniformity.

The final upper limit on ^{210}Bi including statistical and systematical errors added in quadrature is:

$$\text{Rate}(^{210}\text{Bi}) \leq (11.5 \pm 1.3)\,\text{cpd/100t}$$

4. Spectral analysis

We performed a multivariate analysis, simultaneously fitting the energy spectra in the window between 320 keV and 2640 keV and the radial distribution of the selected events, using the data collected from June 2016 to February 2020 (Borexino Phase-III). The fiducial volume (FV) is defined as r<2.8 m and z in the interval (-1.8 m, 2.2 m) (r and z being the reconstructed radial and vertical position, respectively). The total exposure corresponds to 1072 days · 71.3 tonnes. Free parameters in the fit procedure are: the interaction rate of CNO neutrinos, ^{85}Kr, ^{11}C, internal and external ^{40}K, external ^{208}Tl and ^{214}Bi, and ^{7}Be neutrinos. The pep neutrino rate is constrained to to 2.74 ± 0.04 cpd per 100 t by multiplying the standard likelihood with a symmetric Gaussian term. The upper limit to the ^{210}Bi rate is the one reported in previous section. It is enforced asymmetrically by multiplying the likelihood with a half-Gaussian term, i.e., leaving the ^{214}Bi rate unconstrained between 0 and 11.5 cpd per 100 t .

The reference spectral and radial distributions of each signal and background species are obtained with a complete GEANT4-based Monte Carlo simulation which models all physics processes occurring in the scintillator, including energy deposition, photon emission, propagation, and detection, generation and processing of the electronic signal. The simulation takes into account the evolution in time of the detector response and produces data that are reconstructed and selected following the same pipeline of real data. The results of the simultaneous multivariate fit of the energy spectra are given in Fig. 6, showing the TFC subtracted and TFC-tagged data. The fit is performed in the energy estimator N_{hits} (defined as the sum of all photons triggering a PMT, normalized to 2000 active PMTs) and the results are reported also in keV. The p-value of the fit is 0.3, demonstrating fair agreement between data and the underlying fit model. The fit clearly prefers a non-zero CNO neutrino rate as also shown in a detailed study of log-likelihood profile.

The best fit value of the CNO neutrinos interaction rate is 7.2 cpd per 100 t with an asymmetric confidence interval of -1.7 cpd per 100 t and +2.9 cpd per 100 t (68% C.L.), considering the statistical error only. The many details of the analysis, including the list and evaluation of the systematic effects are reported in.[26] Folding the systematic uncertainty over the log-likelihood profile we determine the final CNO interaction rate to be $7.2^{+3}_{-1.7}$ cpd per 100 t. The rate can be converted to of CNO neutrinos on Earth of $7.2^{+3.0}_{-2.0} \cdot 10^8$ cm^{-2} s^{-1} assuming MSW conversion in matter and a density of electrons in the scintillator of $(3.307 \pm 0.015) \cdot 10^{31}$ e$^-$per 100 t.

In order to evaluate the significance of our result in rejecting the no-CNO hypothesis, we performed a frequentist hypothesis test using the profile likelihood.

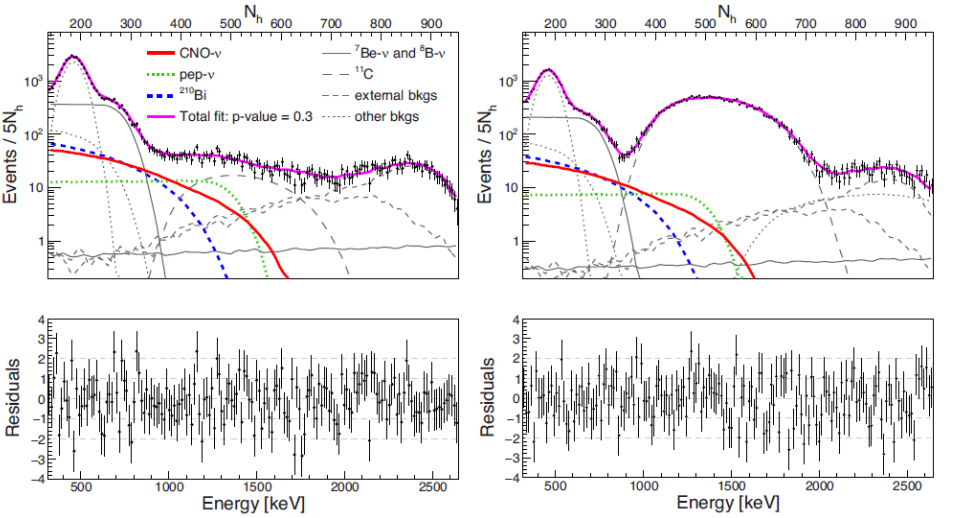

Fig. 6. Energy distributions from a multivariate fit of the Borexino data. Full multivariate fit results for the TFC-subtracted (left) and the TFC-tagged (right) energy spectra with corresponding residuals. In both graphs the magenta lines represent the resulting fit function, the red line is the CNO neutrino electron recoil spectrum, the green dotted line is the pep neutrino electron recoil spectrum, the dashed blue line is the ^{210} β spectrum, and in grey we report the remaining background (bkgs) contributions.

We defined a test statistics q, as the ratio between the maximum likelihood obtained by keeping the CNO rate fixed to zero or free. Figure 7 shows the q distribution obtained from 13.8 millions of pseudo-data sets simulated with deformed PDFs to include systematics effects, and no-CNO injected (q_0, grey curve). In the same plot, the theoretical q_0 distribution in case of no PDF deformation is shown (blue curve). The result on data obtained from the fit is the black line ($q_{data} = 30.05$). The results reported in Figure 7 allow us to reject the CNO = 0 hypothesis with a significance better than 5.0σ at 99.0% C.L. In the figure we also provide as reference the q distribution (red) obtained with one million pseudo-data sets including systematic deformations and injected CNO rate equal to 7.2 cpd per 100 t, i.e., our best fit value.

The results of the analysis based on the fit are also confirmed by that obtained with a nearly independent method (counting analysis), in which we simply count events in an optimized energy window (region of interest, ROI) and subtract the contributions due to known backgrounds. This method reveals a non zero CNO signal and its consistency with the multivariate analysis is remarkable. This method is simpler, albeit less powerful, with respect to the multivariate fit and is less prone to possible correlations between different species. However, while the multivariate analysis implicitly checks the validity of the background model by the goodness of the fit, the counting analysis relies completely on the assumption that there are no unknown backgrounds contributing to the ROI.

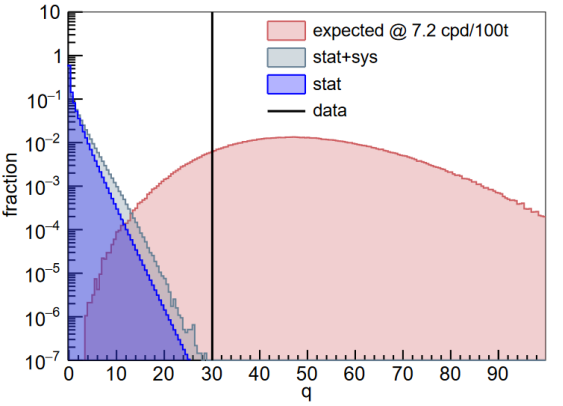

Fig. 7. Distribution of the test statistic q, as discussed in the text.

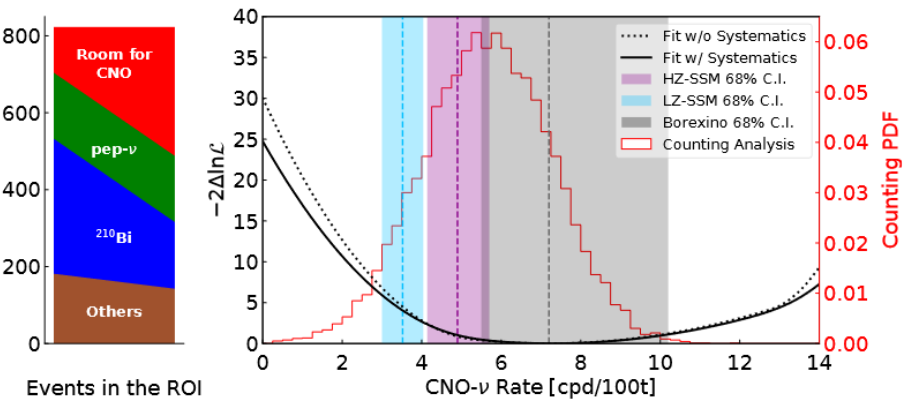

Fig. 8. Results of the CNO counting and spectral analyses. Left. Counting analysis bar chart. The height represents the number of events allowed by the data for CNO neutrinos and backgrounds in the ROI; on the left, the CNO signal is minimum and backgrounds are maximum, while on the right, CNO is maximum and backgrounds are minimum. It is clear from this figure that CNO cannot be zero. Right. CNO neutrinos rate negative log-likelihood profile directly from the multivariate fit (dashed black line) and after folding in the systematic uncertainties (black solid line). Histogram in red: CNO neutrino rate obtained from the counting analysis. Finally, the blue, violet, and grey vertical bands show 68% confidence intervals (C.I.) for the SSM-LZ (3.52±0.52 cpd per 100 t) and SSM-HZ (4.92±0.78 cpd per 100 t) predictions and the Borexino result (corresponding to black solid-line log-likelihood pro- file), respectively.

Conclusions

We have reported the results about the first direct detection of neutrinos from the CNO cycle in the Sun. This result proves the occurrence of the primary mechanism

for the stellar conversion of hydrogen into helium in the Universe. The observation of CNO neutrinos experimentally confirms the overall solar picture and shows that a direct measurement of the metallicity of the Sun's core is within reach of an improved, future measurement.

References

1. J. N. Bahcall, Neutrino Astrophysics, *Cambridge University Press*, 1989.
2. N. Vinyoles, A.M. Serenelli, F.L. Villante, S. Basu, J. Bergström, M.C. Gonzalez-Garcia, M. Maltoni, C. Peña-Garay, and N. Song, *Astrophys. J.*, **835**(2):202, 2017.
3. M. Salaris and S. Cassisi, Evolution of Stars and Stellar Populations, *John Wiley & Sons Ltd.*, 2005.
4. C. Angulo et al., *Nuclear Physics A*, **656**(1):3–183, 1999.
5. M. Agostini et al. (Borexino Collaboration), *Nature*, **562**(7728):505–510, 2018.
6. A. M. Serenelli, W. C. Haxton, and C. Peña-Garay, *The Astrophysical Journal*, **743**(1):24, 2011.
7. G. Bellini et al. [Borexino], Phys. Rev. D **89** (2014).
8. C. Arpesella et al. [Borexino], Phys. Lett. B **658** (2008), 101-108.
9. C. Arpesella et al. [Borexino], Phys. Rev. Lett. **101**(2008), 091302.
10. G. Bellini, et al. [Bore ino], Phys. Rev. Lett. **107** (2011), 141302.
11. M. Agostini et al. [Borexino], Nature **587** (2020), 577-582.
12. Website: `https://www.lngs.infn.it`
13. G. Alimonti et al. [Borexino], Astropart. Phys. **16** (2002), 205-234.
14. H. Back et al. [Borexino], JINST **7** (2012), P10018.
15. G. Bellini et al. [Borexino], Phys. Rev. Lett. **108** (2012), 051302.
16. G. Bellini et al. [Borexino], Nature **512** (2014) no.7515, 383-386.
17. M. Agostini et al. [Borexino], Nature **562** (2018) no.7728, 505-510.
18. M. Agostini et al. [Borexino], Phys. Rev. D **100** (2019) no.8, 082004.
19. M. Agostini et al. [Borexino], Phys. Rev. D **101** (2020) no.6, 062001.
20. A. Vishneva et al. [Borexino], J. Phys. Conf. Ser. **888** (2017), 012193.
21. S. K. Agarwalla et al. [Borexino], JHEP **02** (2020), 038.
22. M. Agostini et al. [Borexino], Astropart. Phys. **125** (2021), 102509.
23. M. Agostini et al. [Borexino], Phys. Rev. D **96** (2017), 091103.
24. G. Bellini et al. [Borexino], Phys. Rev. D **88** (2013), 072010.
25. M. Agostini et al. [Borexino], Phys. Rev. D **101** (2020), 012009.
26. The Borexino Collaboration, *Nature* **587**, 577 (2020).
27. The Borexino Collaboration, *arXiV:2106.1097*. Submitted for publication on *EPJ C*.
28. V. Di Marcello *et al*, *Nucl. Instrum. Meth. A*, **964**, 163801 (2020).